A BUNDLE-SCALE MODEL OF PROPAGATION OF A THROUGH-THE-THICKNESS NOTCH IN A THIN WOVEN COMPOSITE UNDER FATIGUE LOADING

T. Rouault[1,2*], C. Bouvet[1], M. Bizeul[1], V. Nègre[2], P. Rauch[2]

[1]*Université de Toulouse ; ISAE, INSA, UPS, EMAC ; ICA (Institut Clément Ader) ; ISAE, 10 av. E. Belin, 31055 Toulouse, France*
[2] *Eurocopter, 13725 Marignane, France*
**thomas.rouault@isae.fr*

Keywords: thin woven composite, GFRP, through-the-thickness crack, fatigue propagation

Abstract
The propagation of a through-the-thickness crack on woven laminate under high cycle fatigue loading has been simulated using an original modelling based on the bundle scale. The approach developed in this paper is constituted according to experimental observation of damage in woven glass-epoxy fabric. It uses finite element method including semi-discrete damage to represent matrix micro-cracks and cumulative damage law to compute fibres lifetime. The modelling can be applied to planar problems of crack propagation under multi-axial loading. Its results were compared to experimental propagation tests on woven glass-epoxy structural samples.

1 Introduction
Helicopter blades are typically constituted by a stiff spar and a foam filling, covered with thin composite skin. High cycle fatigue loading combined with previous damage can trigger a notch at the trailing edge of the blade. This notch, propagating through the thickness of the laminate is also known as *translaminar* crack [1]. For a failsafe design of blades, the damage phenomena have to be understood and the potential propagation of cracks has to be quantified. It was shown in an experimental study [2] that under fatigue loading, when a translaminar crack propagates, a fibre bundle can only collapse entirely. Thus, the crack propagation speed is strongly dependant on the width of the fibre bundle, and the scale of the modelling was chosen according to this observation. Between the micro-scale approach aiming at representing separately the two components of the material [3], and macro-scale models where properties are homogenized, and continuum damage mechanics is used [4], this paper describes a modelling where the material is meshed according to the bundle width. A semi-discrete damage is implemented in accordance with microscopic analysis. It implies that no sharp crack tip appears but an area where bundles are allowed to softly drift to one another, since in experimental tests, many matrix failures occur at the crack tip. This strategy doesn't match with the use of classical fracture mechanics. Then, a damage law is used to simulate these matrix micro-cracks, and fibres lifetime is predicted by a fatigue curve.
Besides, for the particular application of this study, considering the high stiffness of the spar, displacement field is supposed constant sufficiently far from the crack. Structural tests are

then represented by experimental and numerical strain controlled tests, and the fatigue law we use is an ε-N curve.
A first part describes the way the damage is observable, providing arguments for choices in the modelling approach, which is developed in a second and third section. Finally numerical simulations are compared to experimental results.

2 Study of the damage

The material studied is an 8-harness satin weave glass-epoxy composite. Quasi-static stress-strain responses under tension and shear loading for a $[0/90]_2$ are shown in Figure 1.
An investigation was carried out to characterize damage form for this particular material under cyclic loadings. Several studies describe micro-crack in transverse yarns under quasi-static tension on woven laminates [5] [6]. To compare with fatigue damage form, cyclic tension-tension loadings were applied to samples and fragments were cut out and polished to observe the damaged material with the aid of SEM.

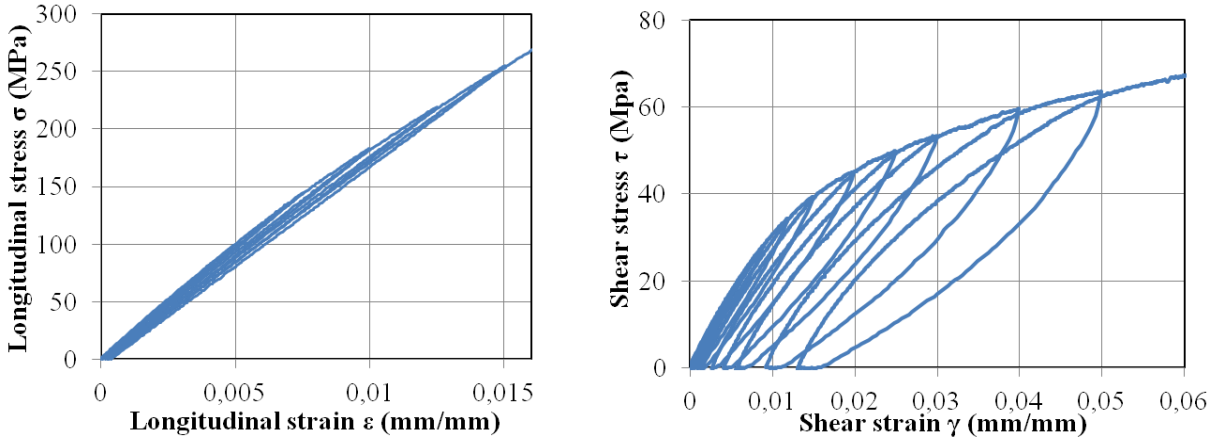

Figure 1. Stress-strain response under tension (left) and shear (right) loading of a $[0/90]_4$ laminate of the studied material. Charge and discharge were applied to evaluate rigidity and inelastic strain evolution.

Figure 2 shows some results of SEM visualisation of a damaged sample through different sections. Damage is found to be similar as in quasi-static, without noticeable crack density increase.

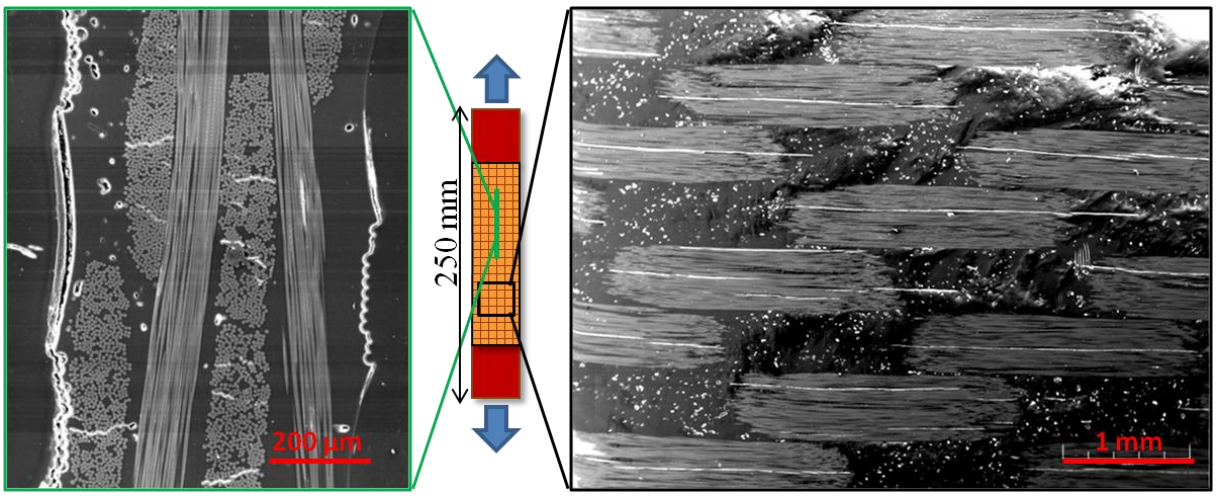

Figure 2. Damage in a woven GFRP under tension-tension fatigue loading after 5.10^4 cycles at 1% maximum longitudinal strain.

The same work was carried out on shear samples. A rail-shear test experiment in accordance with D4255 ASTM norm [7] was used to study the damage on samples under cyclic shear loading. Though we observe a decrease of about 15% of the shear modulus, and we increased the load to high strain (higher than 3%), no SEM observation has revealed any crack (Figure 3) contrary to the tension case. It seems that epoxy resin toughness is much higher in shear than in tension, as already noticed for this type of matrix which toughness is said to be sensitive to the hydrostatic part of the stress tensor [8]. The macroscopic loss of stiffness and inelastic strains are consequently attributed to lower scale matrix damage.

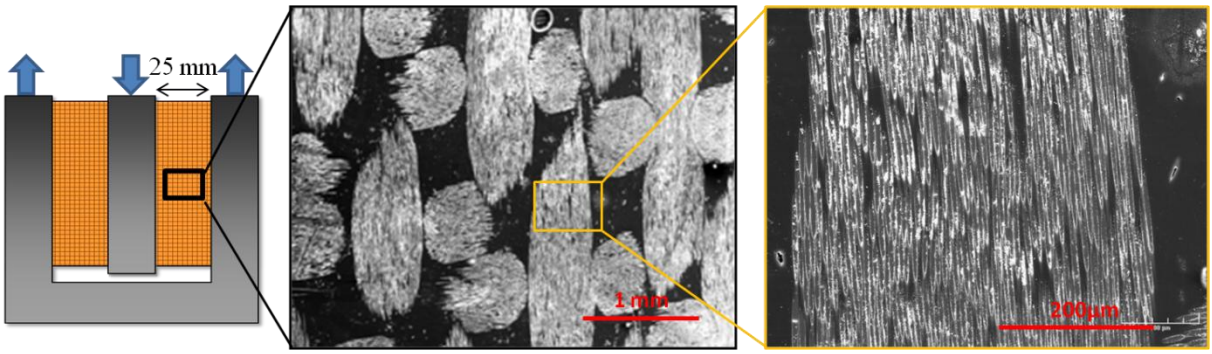

Figure 3. SEM micrography of the surface of a sample after high strain cyclic loading.

3 Modelling approach

A mesh is generated with squared quadrangle elements (Figure 4). Their size is equal to the width of the tow to take into account the scale of bundles into modelling. Each bundle is meshed by a raw of quadrangles linked each other's by interface elements represented as springs as explained in [9] and [10]. These interface elements contain potential damage of the material through their evolving stiffness. They provide a semi-discrete damage, as it is not homogenised. Their stiffness is initially a constant k_0, high enough to be numerically equivalent to infinity, and it can evolve during the test. Finally, failure interface elements simply called "*failure elements*" are added into bundles to ensure crack propagation.

3.1. Matrix damage under tension

SEM observations Figure 2 lead to the choice of modelling tension fatigue damage through interface elements which provide semi-discrete damage. Damage law has been identified on quasi-static and fatigue experiments. Fatigue tests were performed for various amplitude of cyclic imposed strain, characterised by maximum strain ε_{max}, and load ratio $R = \varepsilon_{min} / \varepsilon_{max}$ which is set to 1/3 for every test in order to limit the number of experiments. For fatigue tests, the Young modulus E has been measured and compared to the initial Young modulus E_0 as a function of the number of cycle N. These tests results in a relation between damage d, maximum longitudinal strain, ε_{max}, and the number of cycle:

$$d = 1 - \frac{E}{E_0} = f(\varepsilon_{max}, N) \quad (1)$$

As it is possible to state a relation between d and element stiffness k [2], the last one evolves through this relation and the law (1) which is identified experimentally. The strain ε_{max} considered to compute the stiffness of interface elements is taken from neighbouring quadrangle elements. Experimentally, when strain into bundle exceeds a damage threshold,

micro-cracks develop, resulting in a worse load transmission between bundles. The softening of interface elements aims at simulating this phenomenon.

3.2. Inelastic strains

As shown in Figure 1, no inelastic strains are noticed when the loading is parallel to the direction of reinforcements, whereas under off axis loading, non-linear behaviour, and inelastic strains are observed. As this kind of damage seems to appear diffusely (Figure 3), it has been integrated into quadrangle 2D elements with a pseudo-hardening material law.

3.3. Crack propagation

Generally, the crack path can't be known *a priori*, except for specific conditions (geometrical and material symmetry). Consequently, since previous works [9], failure elements have been introduced into bundles between all the quadrangle elements so that crack can propagate arbitrarily in the direction determined by damage state and strain field.

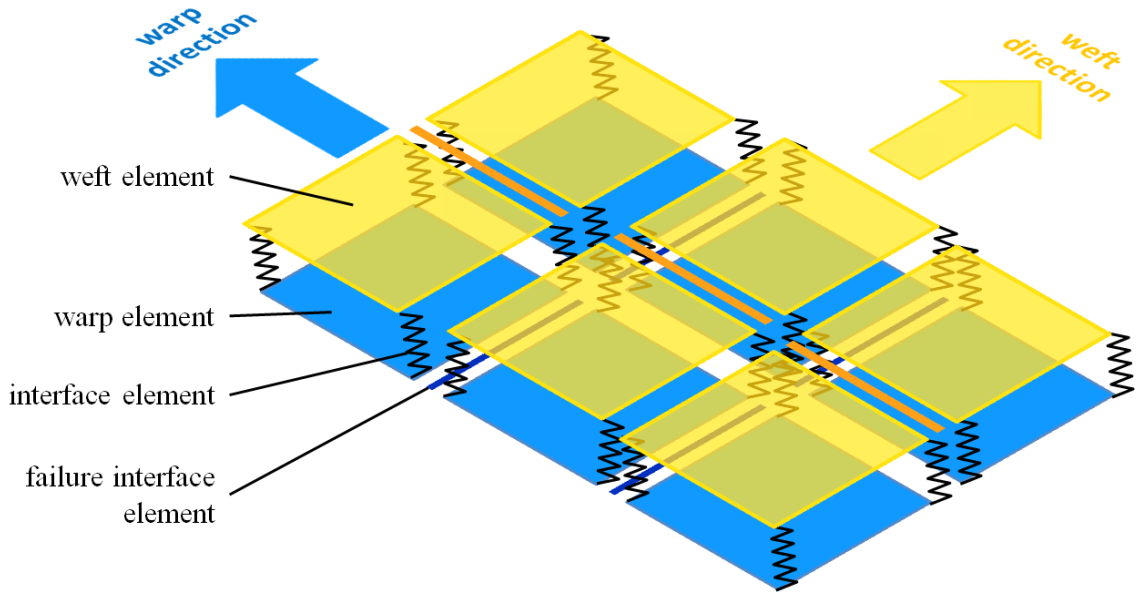

Figure 4. Modelling principle. The two superimposed meshes are represented separately for more clarity. Consequently, spring interface elements and failure elements sizes, is non zero.

For that purpose, a cumulative damage parameter *D(i)* has been affected to each node *i*, and each failure element *j* evolves as a function of cumulative damage $D_j(i)$ of the neighbouring nodes in the neighbouring quadrangle elements. If one of the $D_j(i)$ reaches 1, the failure element collapses. Experimentally, no loss of stiffness is observed in the fibre direction. Thus, a binary behaviour is assigned to failure elements and no stiffness decrease occurs until complete failure:

$$\begin{cases} k(j) = k_0 \; if \; D_j(i) < 1 \\ k(j) = 0 \; if \; D_j(i) = 1 \end{cases} \quad (2)$$

Values of variable *D* are computed using Miner-Palmgreen cumulative damage law even though the use of this law is generally not recommended for composite materials [11], because it doesn't take into account sequence effect for variable cyclic loading. Regarding this law, a low-high sequence and a high-low sequence are supposed to involve the same damage level. The issue of determine which sequence is the most damaging, has been treated

in literature, resulting in divided opinions because authors use different experimental conditions on different materials [12]. As our particular material behaviour is unknown concerning sequence effect, the Miner-Palmgren law has been adopted since its neutrality about this point.
However, as damage is included in interface elements with non-linear law (eq. (1)), after a low-high sequence, damage state is not the same as after a high-low sequence, leading to different strain fields between the two low levels and the two high levels and thus it involves different Miner's fraction of life *D*. Therefore a sequence effect is implicitly represented.
Miner's law needs the definition of a fatigue law ε-N_{fat} (number of cycles to failure versus maximum strain). We fitted it on experimental curve with a Basquin law according to literature:

$$N_{fat}(\varepsilon) = \left(\frac{\varepsilon}{\varepsilon_6}\right)^{\alpha} \tag{3}$$

where ε_6 = 0,00606 and α = 0,149. The scheme of a mesh with 2 warp and 3 weft bundles with interface and failure elements is shown in Figure 4.

4 Performing of the simulation

The mesh defined above is first generated. It includes squared quadrangle elements, interface elements to link warp and weft tows, and failure elements to allow the crack to get an arbitrary shape. A pre-crack is introduced, and boundary conditions are applied. As mentioned before, they consist in imposed displacement for our particular application of rotor blade. Then, the non-linear solver computes each time step, and as the imposed displacement increases, an area close to the crack tip becomes overloaded; the strain exceeds damage threshold and damage are introduced by a decrease of the interface elements stiffness.
At the maximum imposed strain, the number of cycles to failure of the next bundle is estimated, with fraction of life variables *D*. To each node of each element, the strain ε is evaluated, and the corresponding number of cycles to failure N_r is computed:

$$N_r(i) = \big(1 - D(i)\big) N_{fat}(\varepsilon(i)) \tag{4}$$

The element and the node *i0* where the minimum cycle to failure occurs are saved.

$$N_r(i_0) = \min_i\{N_r(i)\} \tag{5}$$

At the next time step, the failure element next to this node of this element is broken. To that purpose, its stiffness matrix is set to zero. The total number of cycle is increased, and the Miner's damage variables are increased by the fraction of life:

$$N_{tot} + N_r(i_0) \rightarrow N_{tot} \tag{6}$$

$$D(i) + \frac{N_r(i)}{N_r(i_0)} \rightarrow D(i) \tag{7}$$

The high strain area before failure is wide enough to put several Miner's damage variable close to 1. In order to avoid that after tow failure these variables involve others failures of the

same tow, interface element stiffness are set to 0 in an area surrounding tow failure, defined as 2 tow widths in the collapsed tow (Figure 5 c).

$$k(j) = 0 \; j \in area\; surrounding\; tow\; failure \tag{8}$$

A scheme of this scenario is shown in Figure 5. Finally the crack path and evolution of N_{tot} are saved for post-processing to compute crack propagation speed.

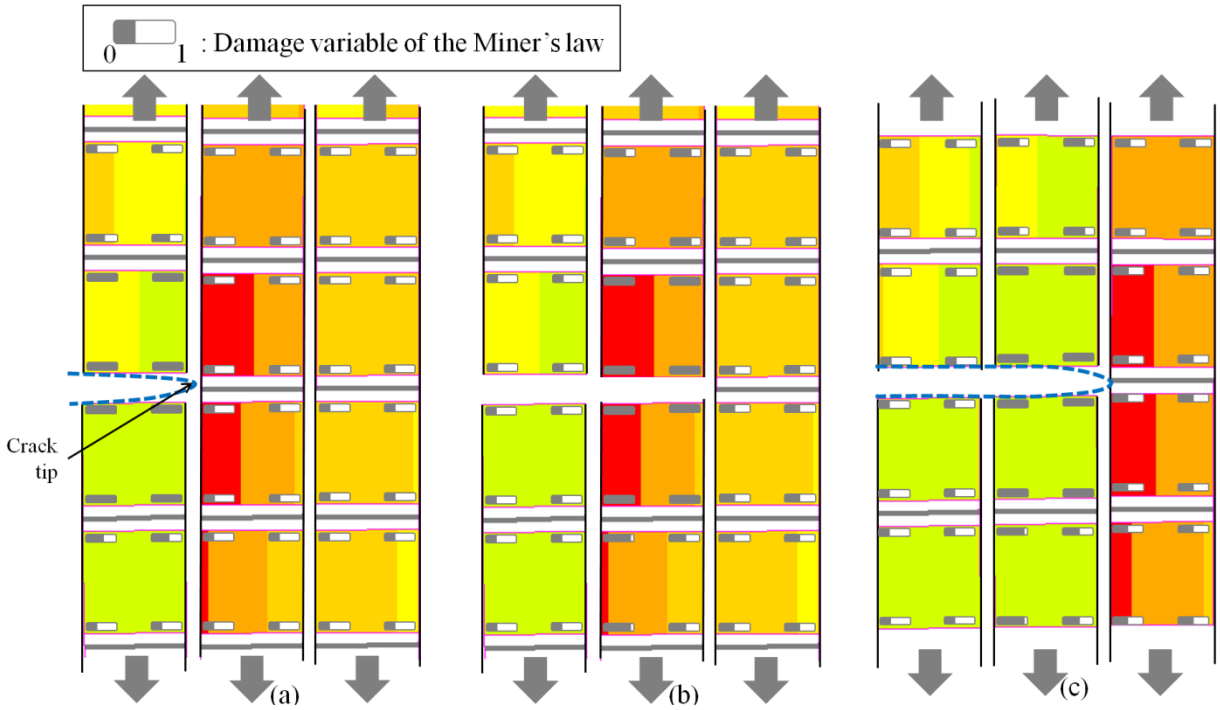

Figure 5. Performing of the simulation, colour gradation represents the longitudinal strain. (a) A static solution of the FE problem is found with non linear solver. It computes the next bundle number of cycles to failure. Fractions of life in the last failed bundle are equal to 1. (b) The failure element is collapsed, and fractions of life are incremented. (c) A new FE problem is solved.

5 Results

This modelling was applied to simulate tension-tension fatigue tests on structural samples based on $[\pm 45]_2$ laminate. The experimental methodology of the test and design of the structural samples are detailed in reference [2].

The Figure 6 shows the warp and weft meshes corresponding to +45° and -45° tows after propagation. The simulated averaged direction of propagation appears to be orthogonal to the tension direction, where there is maximum mode I energy release rate. Thus, the crack propagation breaks up alternatively a warp and a weft tow as noticed on experimental tests.

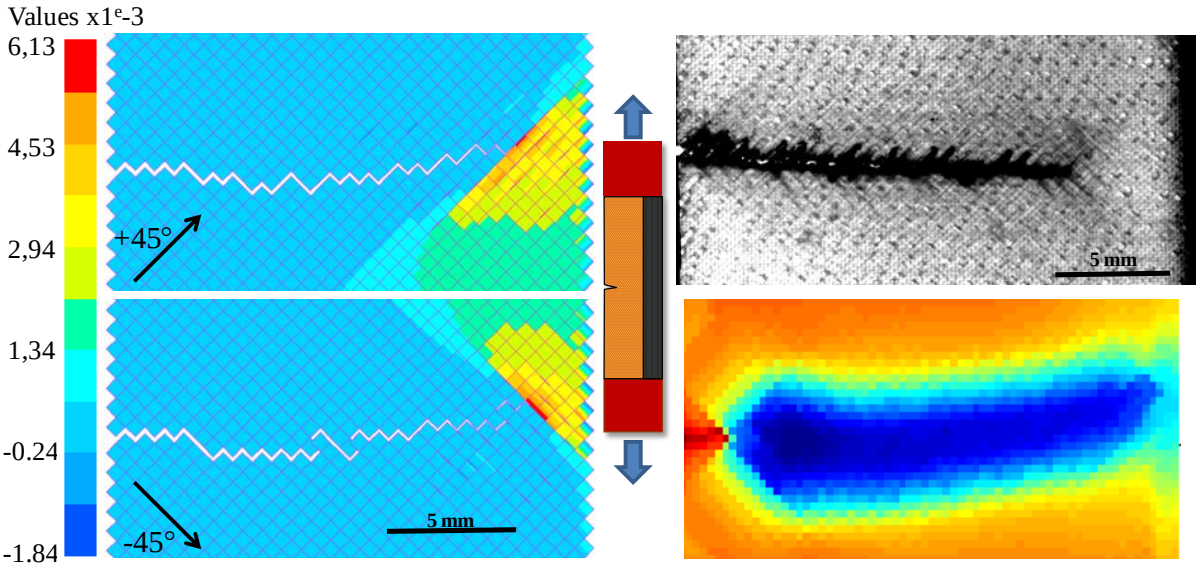

Figure 6. Results for fatigue crack growth on [±45°] structural sample. Left: longitudinal strain computed in warp and weft meshes. Top-Right: photography of an experimental test. Bottom right: interface elements stiffness field around the crack (blue represents zero and red corresponds to k_0).

The numerical damage area can also be evaluated, in plotting the interface elements stiffness field. It can be compared with the top right picture where resin whitening is noticed. It reveals damage matrix area (darker on the picture) of a few millimetres width, at each side of the crack, and dark micro-cracks lines in ±45° direction, parallel to bundles.

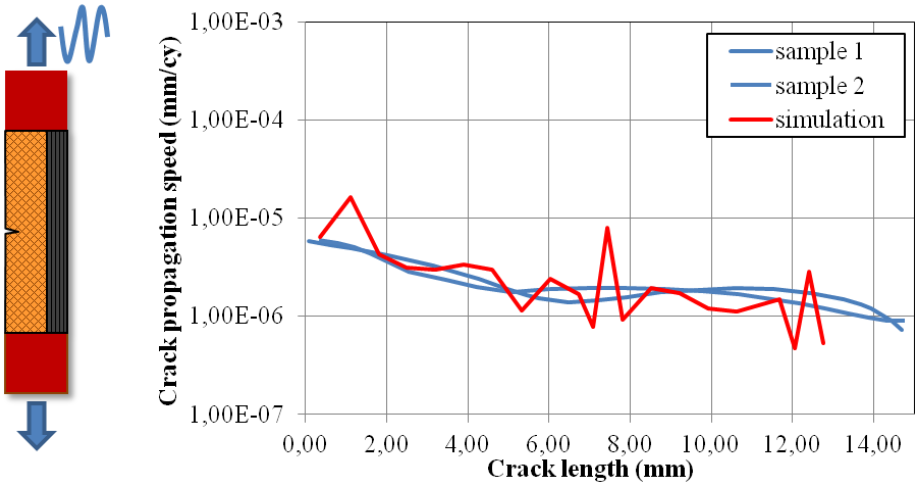

Figure 7. Comparison between experimental and numerical crack propagation speeds.

Crack propagation speed evolution has been computed and compared to experimental one in Figure 7. A good correlation is found as the speed decreases with the development of the crack. However, strong variations are superimposed to the main tendency of the curve. They can be attributed to the severe degradation of interface elements stiffness around failure. Some others phenomenon such as the number of ply effect not considered in this modelling can also be related to this shape of the curve. Others cases have to be evaluated and improvements have to be carried out, to attenuate instabilities.

6 Conclusion

An original approach has been developed to reach the modelling presented above. It is based on phenomenological aspects and experimental considerations. It enables to simulate crack propagation phenomenon, with semi-discrete damage. The simulation has been compared to experimental results under load conditions according to the application of the modelling. It seems to provide good representation of the phenomenon in spite of some lack of confidence in cumulative fatigue laws and some noise in crack propagation speed results. Further developments have to be done to evaluate the performance of the modelling for others load cases.

References

[1] Laffan M. J., Pinho S. T., Robinson P., and McMillan A. J., "Translaminar fracture toughness testing of composites: A review," *Polymer Testing* (2012).

[2] Bizeul M., Bouvet C., Barrau J. J., and Cuenca R., "Fatigue crack growth in thin notched woven glass composites under tensile loading. Part I: Experimental," *Composites Science and Technology* **71**, 289–296 (2011).

[3] Pineau P., Couégnat G., and Lamon J., "Virtual testing applied to transverse multiple cracking of tows in woven ceramic composites," *Mechanics Research Communications*, 38, pp. 579-585 (2011).

[4] Hochard C., Payan J., and Bordreuil C., "A progressive first ply failure model for woven ply CFRP laminates under static and fatigue loads," *International Journal of Fatigue* **28**, pp. 1270–1276 (2006).

[5] Gao F., Boniface L., Ogin S. L., Smith P. A., and Greaves R. P., "Damage accumulation in woven-fabric CFRP laminates under tensile loading: Part 1. Observations of damage accumulation," *Composites Science and Technology* **59**, pp. 123–136 (1999).

[6] Osada T., Nakai A., and Hamada H., "Initial fracture behavior of satin woven fabric composites," *Composite Structures* **61**, pp. 333–339 (2003).

[7] "ASTM D4255/D4255M-83: Standard Guide for Testing In-Plane Shear Properties of Composite Laminates (Two- and Three-Rail Shear Test)" (1994).

[8] Fiedler B., Hojo M., Ochiai S., Schulte K., and Ando M., "Failure behavior of an epoxy matrix under different kinds of static loading," *Composites Science and Technology* **61**, pp. 1615–1624 (2001).

[9] Bizeul M., Bouvet C., Barrau J. J., and Cuenca R., "Fatigue crack growth in thin notched woven glass composites under tensile loading. Part II: Modelling," *Composites Science and Technology* **71**, pp. 297–305 (2011).

[10] Rouault T., Bouvet C., Bizeul M., and Nègre V., "Modélisation de la propagation d'une coupure sur stratifié mince de composite tissé soumis à un chargement cyclique de traction," presented at 17èmes Journées Nationales sur les Composites (JNC17), 15 June 2011, Poitiers-Futuroscope, France.

[11] Post N. L., Case S. W., and Lesko J. J., "Modeling the variable amplitude fatigue of composite materials: A review and evaluation of the state of the art for spectrum loading," *International Journal of Fatigue* **30**, pp 2064–2086 (2008).

[12] Paepegem W. V. and Degrieck J., "Effects of Load Sequence and Block Loading on the Fatigue Response of Fiber-Reinforced Composites," *Mechanics of Advanced Materials and Structures* **9**, pp 19–35 (2002).